\



Probing structural and electronic properties of divalent metal Mg_{n+1} and $SrMg_n$ (n=2-12) clusters and their anions

Song-Guo Xi(奚松国), Qing-Yang Li(李青阳), Yan-Fei Hu(胡燕飞), Yu-Quan Yuan(袁玉全), Ya-Ru Zhao(赵亚儒), Jun-Jie Yuan(袁俊杰), Meng-Chun Li(李孟春), and Yu-Jie Yang(杨雨杰)

Citation: Chin. Phys. B, 2022, 31 (**1**): 016106. DOI: 10.1088/1674-1056/ac04aa
Journal homepage: http://cpb.iphy.ac.cn; http://iopscience.iop.org/cpb

What follows is a list of articles you may be interested in

Growth of PbS nanoclusters on specific sites of programmed oligodeoxynucleotides

Lu Ying, Teng Cui-Juan, Li Ying, Wang Hui, Xu Chun-Hua, Hu Shu-Xin, Li Ming
Chin. Phys. B, 2015, 24 (**1**): 016101. DOI: 10.1088/1674-1056/24/1/016101

Silicon micro-hemispheres with periodic nanoscale rings produced by the laser ablation of single crystalline silicon

Chen Ming, Li Shuang, Cui Qing-Qiang, Liu Xiang-Dong
Chin. Phys. B, 2013, 22 (**10**): 106101. DOI: 10.1088/1674-1056/22/10/106101

High stability of the goldalloy fullerenes:A density functional theory investigation of $M_{12}@Au_{20}$ (M=Na, Al, Ag, Sc, Y, La, Lu, and Au) clusters

Zhang Meng,Feng Xiao-Juan,Zhao Li-Xia,Zhang Hong-Yu,Luo You-Hua
Chin. Phys. B, 2012, 21 (**5**): 056102. DOI: 10.1088/1674-1056/21/5/056102

Hcp-icosahedron structural transformation induced by the change in Ag concentration during the freezing of $(CoAg)_{561}$ clusters

Xiao Xu-Yang
Chin. Phys. B, 2012, 21 (**4**): 046102. DOI: 10.1088/1674-1056/21/4/046102

Probing structural and electronic properties of divalent metal Mg_{n+1} and $SrMg_n$ ($n = 2$–12) clusters and their anions

Song-Guo Xi(奚松国)[1], Qing-Yang Li(李青阳)[1], Yan-Fei Hu(胡燕飞)[2], Yu-Quan Yuan(袁玉全)[1,†], Ya-Ru Zhao(赵亚儒)[3], Jun-Jie Yuan(袁俊杰)[1], Meng-Chun Li(李孟春)[1], and Yu-Jie Yang(杨雨杰)[1]

[1] *School of Physics and Electronic Engineering, Sichuan University of Science & Engineering, Zigong* 643000, *China*
[2] *Department of Applied Physics, Chengdu University of Technology, Chengdu* 610059, *China*
[3] *College of Physics & Optoelectronics Technology, Baoji University of Arts and Sciences, Baoji* 721016, *China*

(Received 7 March 2021; revised manuscript received 19 May 2021; accepted manuscript online 25 May 2021)

Divalent metal clusters have received great attention due to the interesting size-induced nonmetal-to-metal transition and fascinating properties dependent on cluster size, shape, and doping. In this work, the combination of the CALYPSO code and density functional theory (DFT) optimization is employed to explore the structural properties of neutral and anionic Mg_{n+1} and $SrMg_n$ ($n = 2$–12) clusters. The results exhibit that as the atomic number of Mg increases, Sr atoms are more likely to replace Mg atoms located in the skeleton convex cap. By analyzing the binding energy, second-order energy difference and the charge transfer, it can be found the $SrMg_9$ cluster with tower framework presents outstanding stability in a studied size range. Further, bonding characteristic analysis reveals that the stability of $SrMg_9$ can be improved due to the strong s–p interaction among the atomic orbitals of Sr and Mg atoms.

Keywords: $SrMg_n$ ($n = 2$–12) clusters, CALYPSO code, density functional theory (DFT) optimization

PACS: 61.46.Bc **DOI:** 10.1088/1674-1056/ac04aa

1. Introduction

During the past decades, owing to the special structure and bonding properties, a great many of studies on magnesium (Mg) clusters have been conducted theoretically and experimentally.[1–7] It is worth mentioning that density functional theory (DFT) with appropriate functional and basis sets is known as an efficient method for clustering study.[8–11] Taking the research of neutral and charged Mg_n clusters for example, Xia *et al.*[6] studied the aromatic homonuclear Mg_{17} cluster by using the B3PW91 functional with the 6-311+G(d) basis set, and their results displayed that the Mg_{17} cluster is the first neutral locally π-aromatic homonuclear all-metal cluster. Belyaev *et al.*[7] reported the electronic, spectral, structural, and thermodynamic characteristics of Mg_n ($n = 2$–31) clusters at B3PW91/6-31G (d), B3PW91/6-311+G (2d) set levels, then they revealed that in the range of Mg_2–Mg_{31}, the atomization energy and band gap energy have significant non-monotonic changes, and gradually approach to the atomization energy and band gap energy of ideal metal.

In recent years, there have been many studies on doping clusters.[12–20] Wang *et al.*[12] investigated Au_nM_2 ($n = 1$–6, $M =$ Ni, Pd, and Pt) clusters and found that the average atomic binding energies of this clusters are close to a limit, which is in a range of 1.56 eV–2.00 eV. Kuang *et al.*[13] discussed the DFT results of Au_nAg ($n = 1$–12) clusters and discovered that all the Au_nAg ($n = 1$–12) clusters prefer low spin multiplicity. For Mg cluster doping, Zhu *et al.*[14] employed the DFT method of $SiMg_n$ ($n = 1$–12) clusters with B3LYP/6-311G(d) and found that $SiMg_5$ and $SiMg_8$ clusters were more stable than other clusters. Zhang *et al.*[15] used the DFT method of Be_2Mg_n ($n = 1$–20) clusters with B3PW91/6-31G and found that Be_2Mg_8 cluster is the most stable. To the best of our knowledge, there are few researches on strontium (Sr)-doped Mg clusters. So we hope this theoretical calculation can provide some references for subsequent studies.

Sr is a silver-white alkaline earth metal with yellow luster. Owing to its soft texture, Sr has good conductivity for heat, and it can also be used to make alloy, photocell and lighting material because of its active chemical properties. The Mg–Sr is a common binary alloy constituted by Mg and alkali earth elements, and possesses important applications in various fields, such as biodegradable metallic materials. Gu *et al.*[21] studied the binary Mg–Sr alloy systems in the as-rolled state as biodegradable materials for skeletal applications. Bornapour *et al.*[22] reported that the Mg–0.5Sr alloy increases the vitality of human umbilical vein endothelial cells and showed a lower risk of thrombosis than WE43 stent. Comparing with other alkaline earth metals, the electronic properties of $SrMg_n$ clusters are still lacking in systematic analysis. Some essential questions arise as follows. (i) Of the anionic and neutral $SrMg_n$ clusters, which structure is the most stable? (ii) If Sr atoms are doped into Mg_n clusters, will the clusters produce strange structures? (iii) Will delocalized bonding occur when Sr atoms are involved? To reveal these problems, article warm ptimization algorithm combined with DFT is adopted to probe

†Corresponding author. E-mail: yuquan_yuan@suse.edu.cn
© 2022 Chinese Physical Society and IOP Publishing Ltd

the cluster structure, and the most stable structure of $SrMg_n^{0/-}$ clusters was studied in detail. Next, the PES simulation of $SrMg_n^-$ clusters is discussed. The stability, electronic properties and bonding properties of the anionic and neutral $SrMg_n$ clusters are analyzed in detail. We hope that these results in this work can provide some valuable guidelines for the subsequent theoretical and experimental researches about Sr-doped magnesium materials.

2. Computational detail

In this work, the CALYPSO code[23,24] which relies only on the chemical composition and can quickly predict the low-value isomers of the cluster by the particle swarm optimization algorithm is employed to acquire the most stable structure of $Mg_n^{0/-}$ and $SrMg_n^{0/-}$ clusters. Many researches have demonstrated that this method is effective and reliable for cluster structure prediction.[25–32] For getting the variable structures of $Mg_n^{0/-}$ and $SrMg_n^{0/-}$ clusters, we perform 50 generations to achieve the converged structure, including 30 structures for each generation, 80% of which are generated by PSO algorithm and the remaining are generated randomly. Then 1500 structures of variable isomers can be obtained for each of $Mg_n^{0/-}$ and $SrMg_n^{0/-}$. Considering that there have been seldom researches of Sr–Mg system with DFT framework, we conducte a series of tests to obtain the suitable functional method, and we also find that the B3PW91 method is the most suitable for Sr–Mg system. In order to save computing resources, the fundamental energy computations and geometric optimizations of the above-mentioned isomers are performed at the B3PW91/3-21G level. Then, the top 100 lower energy isomers are picked out as the initial configurations to re-optimize at the B3PW91/LANL2DZ level[33] for Sr and B3PW91/6-311+G(d) level[34] for Mg implemented by the Gaussian09 program package.[35] The influence of the spin multiplicity has also been fully considered. Considering the fact that the orbital components need analyzing, the GENECP-labeled basis set is a combination of 6-311+G(d) basis set[34] and SDD [36] basis set for the Mg atom and Sr atom, respectively. Furthermore, the charge transfers among Sr and Mg atoms, the analysis of the bonding features, as well as the simulated PES of anionic clusters based on the Koopman theorem[37] are studied in detail with the assistance of Multiwfn program[38] including the method of adaptive natural density partitioning (AdNDP).[39]

3. Results and discussion

3.1. Geometric structure

Figure 1 displays the most stable structures of the neutral and anionic Mg_{n+1} and $SrMg_n$ (n = 2–12) clusters. The corresponding electronic states and symmetries are listed in Table 1. For investigating the influnces of Sr atom doping on Mg clusters, we first discuss the pure Mg clusters. Notably, the most stable structures (shown in Fig. 1) of Mg_n clusters in our computation are consistent well with the results reported previously.[40–42] All of these show that the functional and basis sets adopted in our work for magnesium and doped magnesium clusters are reliable.

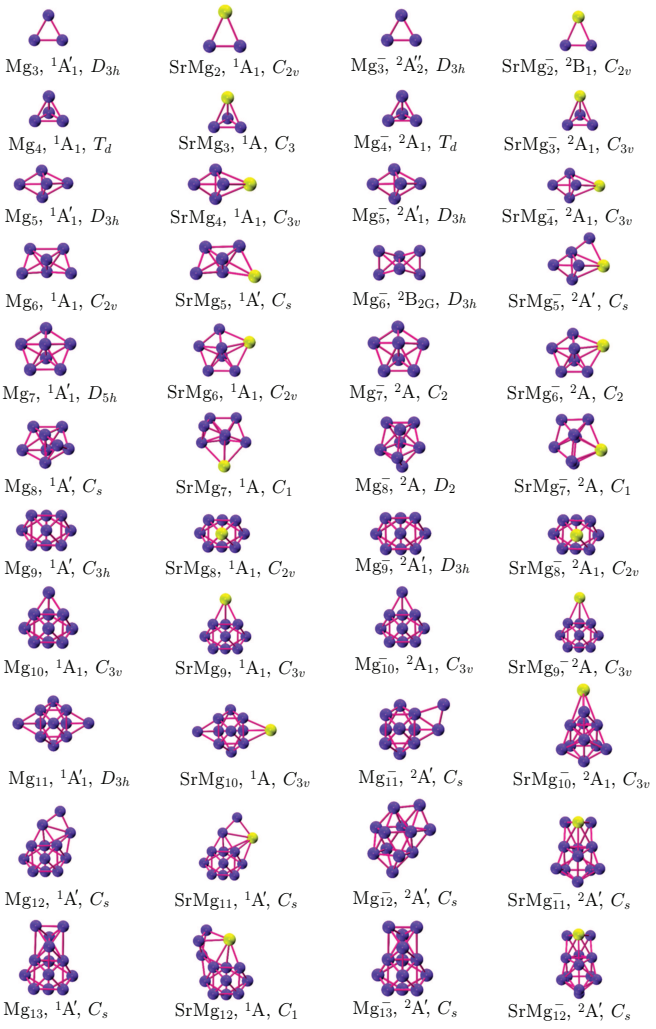


Fig. 1. Global minimum structures of neutral and anionic Mg_{n+1} and $SrMg_n$ (n = 2–12) clusters.

For Sr-doped magnesium clusters, both the neutral and the anionic $SrMg_n$ clusters, the transition point from two-dimensional (2D) to three-dimensional (3D) is $n = 3$, which is consistent with the counterpart for pure Mg clusters. The most stable isomers of neutral and anionic $SrMg_{2-4}$ clusters show identical geometries, which can be viewed as the substituted structures of corresponding pure magnesium clusters. Meanwhile, they can also be generated by adding one Mg atom into the previous cluster. However, for $SrMg_5$ clusters, the configurations of the neutral and anionic species are a little bit different from each orther because Mg atoms cap the different sites of the $SrMg_4$ cluster. When Mg atom caps $SrMg_{n-1}^{0/-}$ clusters, the most stable isomers of the $SrMg_n^{0/-}$ clusters can be yielded at $n = 6$ and 7. Like the pure Mg clusters, the

six-atom triangular prism as a common unit can be found in $SrMg_n^{0/-}$ cluster with size $n = 8$. In other words, a structural reconstruction takes place from $n = 8$. Consequently, most of the $SrMg_{9-12}^{0/-}$ structures are built on the basis of the triangular prism. The typical examples are $SrMg_9^{0/-}$, $SrMg_{10}$, and $SrMg_{11}$ clusters, in which one of the Mg atoms in Mg cluster is replaced by Sr atom. After one Mg atom caps $SrMg_{11}$, the most stable isomer of $SrMg_{12}$ is generated. Obviously, the geometry of the anionic $SrMg_{10-12}$ is different from that of the pure Mg cluster. The growth pattern can be described as clusters of the latter size generated by adding an Mg atom into the structure of the former one. In summary, the Sr doped Mg clusters may keep the original structures of the corresponding Mg clusters except for $SrMg_{12}$, and $SrMg_{5,10\sim12}^-$ clusters. It is clear that the Sr atoms prefer to occupy the convex capped sites of the $SrMg_n^{0/-}$ clusters. The geometries of the neutral $SrMg_n$ clusters are different from those of the corresponding anionic species at $n = 5$, 10, 11, and 12.

Table 1. Electronic states, symmetries, average binding energies E_b (in unit eV), highest occupied molecular orbital and lowest unoccupied molecular orbital (HOMO–LUMO) energy gaps E_g (in unit eV), and charges on Sr atoms of most stable $SrMg_n^{0/-}$ ($n = 2$–12) clusters.

	$SrMg_n$					$SrMg_n^-$				
Clusters	State	Symmetry	E_b	E_g	Charge on Sr	State	Symmetry	E_b	E_g	Charge on Sr
$n = 2$	$^1A_1$	C_{2v}	0.130	2.243	0.175	$^2B_1$	C_{2v}	0.432	0.987	–0.090
$n = 3$	$^1A_1$	C_{3v}	0.282	2.276	0.373	$^2A_1$	C_{3v}	0.548	1.067	–0.015
$n = 4$	$^1A_1$	C_{3v}	0.313	1.773	0.256	$^2A_1$	C_{3v}	0.551	1.061	0.012
$n = 5$	$^1A'$	C_s	0.319	1.764	0.335	$^2A'$	C_s	0.539	1.040	0.159
$n = 6$	$^1A_1$	C_{2v}	0.371	1.722	0.375	^2A	C_2	0.580	1.133	0.167
$n = 7$	^1A	C_1	0.403	1.660	0.454	^2A	C_1	0.613	1.097	0.208
$n = 8$	$^1A_1$	C_{2v}	0.469	1.457	0.570	$^2A_1$	C_{2v}	0.683	1.173	0.352
$n = 9$	$^1A_1$	C_{3v}	0.541	1.641	0.822	$^2A_1$	C_{3v}	0.718	1.122	0.430
$n = 10$	$^1A_1$	C_{3v}	0.538	1.705	0.599	$^2A_1$	C_{3v}	0.689	1.053	0.273
$n = 11$	$^1A'$	C_s	0.528	1.340	0.483	$^2A'$	C_s	0.680	1.045	0.457
$n = 12$	^1A	C_1	0.546	1.431	0.670	$^2A'$	C_s	0.693	1.047	0.464

3.2. Photoelectron spectra of anionic Mg_n and $SrMg_n$ clusters

It is well known that the comparison between the theoretical photoelectron spectra (PES) and the experimental PES is an effective way to verify the reliability of theoretical computation for cluster.[6] Therefore, in Figs. 2 and 3, we present the simulated PES for great majority Mg_n^- and $SrMg_n^-$ clusters and the available experimental PES. The PES are simulated in an energy range of 0 eV–6 eV. Figure 2 shows that the simulated PES of our lowest energy isomers Mg_n^- are consistent with the experimental results, which indicates that the method employed in this work is reliable. From Fig. 3, the simulated PES of $SrMg_2^-$ cluster includes two sets of bimanals, which are 1.87, 2.32, and 4.24, 4.50, respectively, as well as a major spike at 0.79 eV in which the binding energy of the first peak (X) is in agreement with the vertical detachment energy (VDE) value of the $SrMg_2^-$ cluster. With regard to $SrMg_3^-$ cluster, some significant peaks at 0.93 eV, 2.56 eV, and 5.30 eV are existent. The VDE value of $SrMg_4^-$ is 1.07 eV, which is the first peak (X) shown in the simulated spectrum. Following this peak, other peaks are centered at 1.90, 2.93, and 3.38 eV. In addition, the simulated PES of $SrMg_5^-$ cluster display a weak first peak at 1.26 eV, six peaks concentrate in a range of 1.97 eV–4.18 eV. As for $SrMg_6^-$, after the first peak (X) at 1.43 eV, the second strong peak concentrates at 2.10 eV, the others (3th–8th peaks) are located at 2.34, 3.16, 3.50, 4.08, 4.64, and 4.86 eV. The VDE value of $SrMg_7^-$ cluster is 1.70 eV, followed closely by the strong second peak at 2.40 eV. The $SrMg_7^-$ has two attenuation peaks at 4.14 eV and 5.21 eV. The VDE value of $SrMg_8^-$ cluster is centered at 1.84 eV, shown by the position of X, and the binding energies of the other peaks are 2.41, 4.63, and 5.12 eV, respectively. The identical first peaks (X) with 1.70 eV are found in the simulated spectra of $SrMg_7^-$ and $SrMg_9^-$. In addition, the other two single peaks of $SrMg_9^-$ are centered at 2.72 eV and 5.31 eV. In Fig. 3, when the number of Mg atoms is more than 8, the photoelectron spectrum of $SrMg_n^-$ shows more complexity. The $SrMg_{10}^-$ cluster includes two weak peaks located at 1.60 eV (X) and 3.93 eV, and two intense peaks center at 2.89 eV and 5.56 eV. For $SrMg_{10}^-$ cluster, the position of X represents the VDE value (2.00 eV), and $SrMg_{11}^-$ includes the other five peaks located at 2.71, 3.12, 3.87, 4.52, and 5.46 eV. The VDE of $SrMg_{12}^-$ is 2.09 eV, which is shown by the position of X. The next five peaks are observed at 2.36, 2.90, 3.90, 4.92, 4.98, and 5.53 eV, respectively.

Table 2 displays the VDE values of Mg_n^- ($n = 3$–13) and $SrMg_n^-$ ($n = 2$–12) clusters from the PES of Figs. 2 and 3. From Table 2, we can see that the corresponding values of VDE of $SrMg_n^-$ when $n = 2$–8 are smaller than those of Mg_n^-, whereas when $n = 9$, 11, 12, the corresponding values of VDE of $SrMg_n^-$ are larger than those of Mg_n^-.

What is worth mentioning is that there are few reports about the experimental PES of $SrMg_n^-$ clusters. Because of this, we hope that the theoretical PES in this paper can be used to identify the structure of the $SrMg_n^-$ clusters.

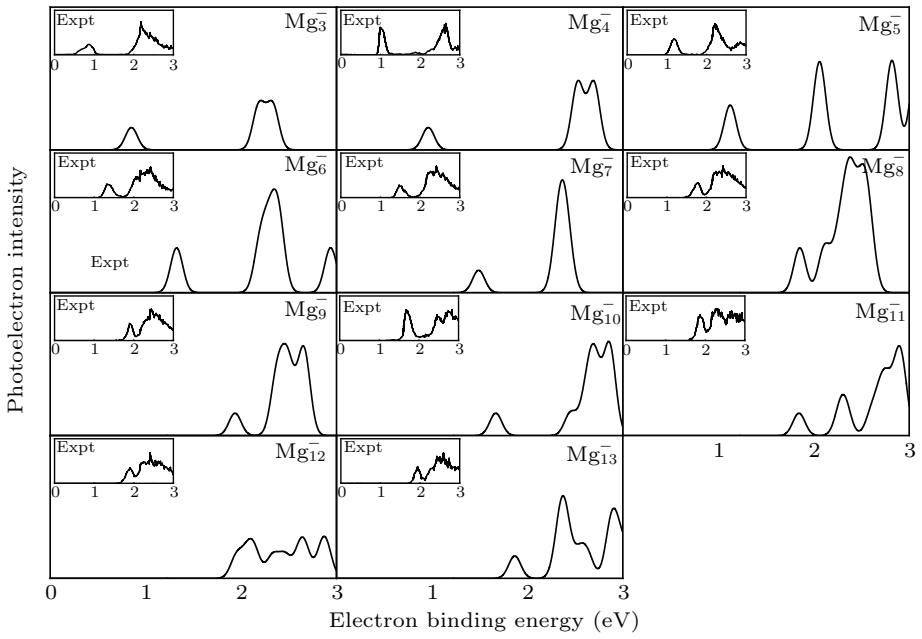


Fig. 2. Comparison between simulated PES and the experimental results for the most stable Mg_n^- clusters.

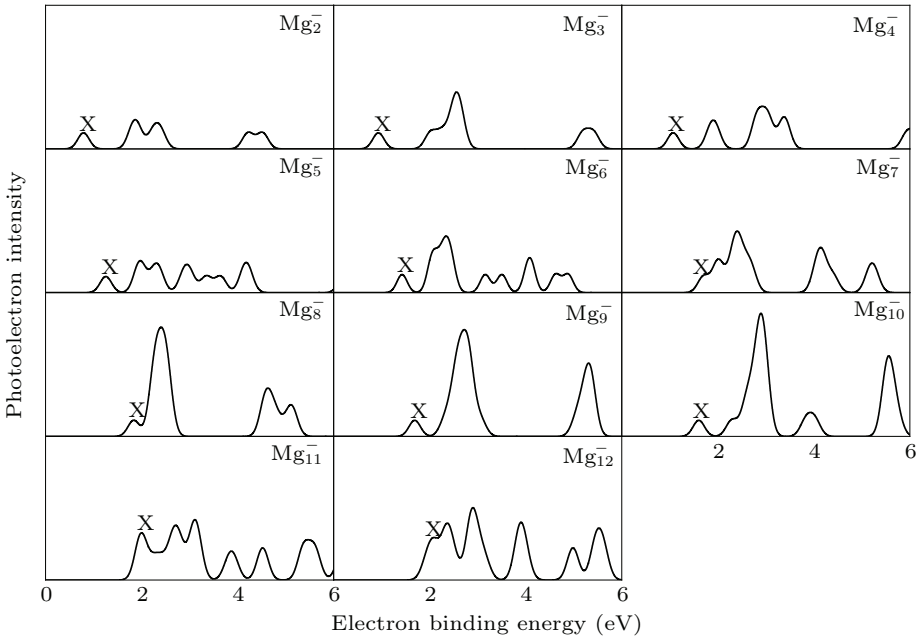


Fig. 3. Simulated PES of the most stable $SrMg_n^-$ clusters.

Table 2. VDE values of Mg_n^- ($n = 3$–13) and $SrMg_n^-$ ($n = 2$–12) clusters (in unit eV).

Mg_n^-		$SrMg_n^-$	
Clusters	VDE	Clusters	VDE
$n = 3$	0.85	$n = 2$	0.79
$n = 4$	0.96	$n = 3$	0.93
$n = 5$	1.13	$n = 4$	1.07
$n = 6$	1.54	$n = 5$	1.26
$n = 7$	1.52	$n = 6$	1.43
$n = 8$	1.85	$n = 7$	1.70
$n = 9$	1.94	$n = 8$	1.84
$n = 10$	1.67	$n = 9$	1.70
$n = 11$	1.87	$n = 10$	1.60
$n = 12$	1.80	$n = 11$	1.94
$n = 13$	1.87	$n = 12$	2.09

3.3. Size-dependent relative stability

For the cluster science, the intrinsic stability of cluster can be expressed by the mean binding energy (E_b) and the second-order energy difference ($\Delta^2 E$). For $SrMg_n^{0/-}$ ($n = 2$–12) clusters, the E_b and $\Delta^2 E$ can be expressed as the following expressions:

$$E_b(SrMg_n^{0/-}) = \frac{(n-1)E(Mg) + E(Mg^{0/-}) + E(Sr) - E(SrMg_n^{0/-})}{n+1}, \quad (1)$$

$$\Delta^2 E(SrMg_n^{0/-}) = E(SrMg_{n-1}^{0/-}) + E(SrMg_{n+1}^{0/-}) - 2E(SrMg_n^{0/-}), \quad (2)$$

where E represents the total energy of the relevant clusters or atoms. According to the aforesaid formula, the specific calculated results are displayed in Fig. 4. The E_b which refers to the average binding energy of clusters is the basis of reflecting the stability of clusters.[43–49] That is to say, the higher the value of E_b, the higher the stability is. From Fig. 4(a) it follows that the values of E_b of anionic clusters are distinctly higher than those of neutral clusters. Furthermore, the E_b values of anionic and neutral clusters increase monotonically, when n is from 3 to 9.

The total energy of the second-order difference clusters can indicate the stability of clusters.[50–55] The larger the value, the more stable it is. As shown in Fig. 4(b), the calculated Δ^2E values suggest that anionic $SrMg_3^-$, $SrMg_6^-$ and $SrMg_9^-$ clusters as well as neutral $SrMg_3$, $SrMg_6$ and $SrMg_9$ clusters are in possession of more distinct stability than their adjacent clusters.

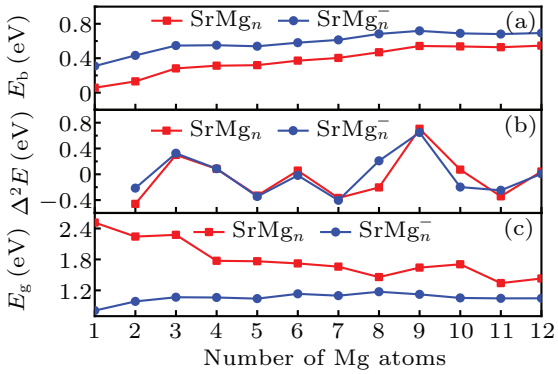


Fig. 4. Size-dependent (a) average binding energy E_b, (b) second-order difference of energy Δ^2E, and (c) HOMO–LUMO energy gap E_g for $SrMg_n^{0/-}$ (n = 1–12) clusters.

The HOMO–LUMO (highest occupied molecular orbital–lowest unoccupied molecular orbital) gap, which is difined as the energy gap between the highest occupied and the lowest unoccupied molecular orbitals, can represent the ability of a molecule to participate in a chemical reaction to some degree. A large value of the HOMO–LUMO energy gap is related to an enhanced chemical stability. Figure 4(c) exhibits the calculated values of the gap E_g of the $SrMg_n^{0/-}$ (n = 1–12) in detail, where E_g represents the HOMO–LUMO gap. Obviously, the simulated results of E_g in both neutral and anionic $SrMg_n$ clusters depend heavily on the size of the cluster. It can be clearly seen that the values of gaps between the anionic $SrMg_n$ are inferior to those of the corresponding neutral $SrMg_n$ clusters. The HOMO–LUMO gap for neutral species reaches its maximum values when n = 1, 3, and 10, indicating that it is more chemically stable. In the range of n = 5–12, the evolution of E_g of the anionic $SrMg_n$ cluster is oscillating compared with that of the neutral cluster due to the presence of extra electrons.

3.4. Charge transfer

The analysis of the charge distribution on atoms can conduce to exploring the mechanism of charge transfer among the atoms of cluster.[56–58] In order to investigate the charge transfer between Sr and Mg atoms for the lowest energy structures of $SrMg_n^{0/-}$ (n = 2–12) clusters, natural population analysis (NPA)[59] is employed to obtain the charge on each atom of $SrMg_n^{0/-}$ (n = 2–12) clusters. The results are presented in Fig. 5. From Fig. 5, we can see that the Sr atoms in the neutral $SrMg_n$ clusters are positively charged within the scope from 0.17 to 0.82 electrons, meaning that the charge in the neutral $SrMg_n$ clusters is transferred from the Sr atom to Mg frame, that is to say, Sr serves as an electron donor in all $SrMg_n$ clusters. The above phenomenon may occur because the electronegativity of Sr atom (0.95) is smaller than the electronegativity of Mg atom (1.31), which implies that the Mg atom is more capable of attracting electrons. The Sr atoms of the anionic $SrMg_n^-$ clusters are negative when n = 1–2, while they are positive when n = 3–12, indicating that the direction of charge transfer will change at n = 3. The value is almost zero in $SrMg_3$ cluster, showing that it is nearly no charge transfer from Sr to Mg atom in this case. Moreover, it is interesting that both neutral and anion $SrMg_9$ clusters have local maximum values. Combining the results of relative stability analysis in the previous section, we conclude that both $SrMg_9$ neutral and $SrMg_9^-$ anion have high stability.

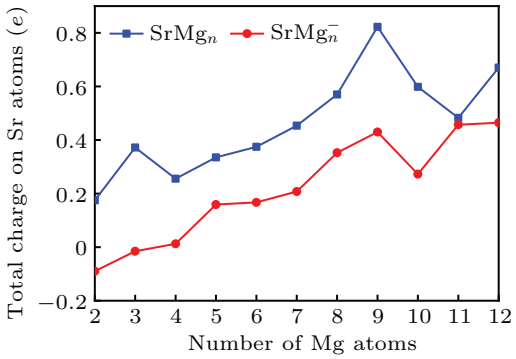


Fig. 5. Size-dependent total charge on Sr atoms for both neutral and anionic $SrMg_n$ clusters.

3.5. Bonding characters

The analyses of molecular orbital, multi-center, bond, and bond order are of great significance in characterizing the bonding characteristics of clusters. Based on the previous discussion, the neutral $SrMg_9$ cluster which has a higher stability is selected as a representative example to detect bonding characteristics. Figure 6 shows the HOMO–LUMO gaps, molecular orbitals and the energy levels of the neutral $SrMg_9$ cluster. The HOMO energy is 1.64 eV lower than the LUMO energy for $SrMg_9$ cluster. The HOMO composition includes 22.97%

of s atomic orbital (AO) of Sr atom and 29.43% of s AO together with 38.144% of p AO of Mg atom. The components of LUMO mainly include 37.53% Sr-s AO, 11.46% Sr-p AO, 9.56% Mg-s AO, and 30.80% Mg-p AO.

In order to further understand the bonding characteristics of the $SrMg_9$ cluster, the adaptive natural density partitioning (AdNDP) method which is particularly suitable to investigating the nature of the chemical bond, is ultilized to study n central double electron (nc–2e) bond systematically, where it can be considered to be delocalized if n is greater than 2, otherwise it is a localized bond when $n = 1$ or 2. The structural diagrams with atomic markers, multicenter bonds, and occupation numbers (ONs) of $SrMg_9$ cluster are displayed in Figs. 7(a) and 7(b), respectively. From Fig. 7(b), seven 4c–2e σ-type bonds with bond orders of 0.3798, 0.2114, 0.3867, 0.3867, 0.2114, 0.2114, and 0.2114 are formed by the 1–3–4–9 $SrMg_3$ unit (ON = 1.95$|e|$) as well as the 7–9–5–10, 7–9–5–5, 3–6–10–8, 3–6–10–6, 4–8–10–6, 4–8–10–6 Mg_4 unit (ON = 1.87$|e|$). In addition, there are three 6c–2e π-type bonds with ON = 1.84$|e|$ in $SrMg_9$ cluster. Their multi-center bond orders are 0.3757, 0.3725, and 0.3725, respectively. For the Sr–Mg bond (ON = 1.95$|e|$), the interaction between Sr and Mg is dominated mainly by the 5s orbital of Sr atom and the 3p, 3s orbitals of the Mg atoms. The Mg–Mg bonds are formed mainly by the 3s orbitals and relatively a small number of 3p orbitals of the Mg atoms, for the other 4c–2e bonds. For three 6c–2e bonds, the interaction of Mg–Mg originates from the 3s and 3p orbitals of Mg atoms. It is worth noting that non localized bond is found in $SrMg_9$ cluster.

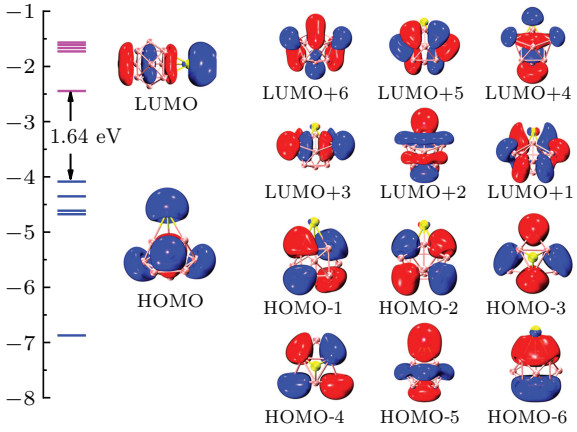


Fig. 6. Molecular orbitals and energy levels of neutral $SrMg_9$ cluster, with HOMO–LUMO gap being denoted in black.

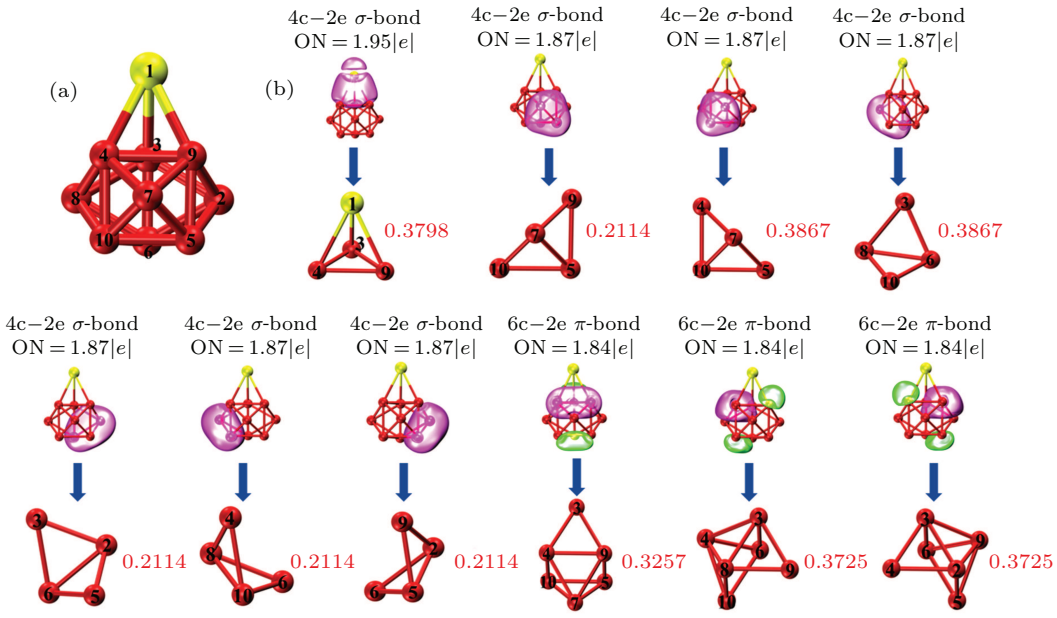


Fig. 7. Analyses of (a) structural diagram with all atomic labels and (b) AdNDP chemical bonds and multi-center bond orders with occupation number (ON) for $SrMg_9$ cluster.

4. Conclusions

The geometric structures and electronic properties of $SrMg_n^{0/-}$ (n = 2–12) clusters are systematically investigated by using the CALYPSO structure prediction code combined with DFT calculations. A great many of low energetic isomers are converged and the most stable structures are confirmed by comparing their total energies for different cluster sizes of the $SrMg_n^{0/-}$ (n = 2–12). For the most stable structure, the transition point from 2D to 3D occurs at $n = 3$, which is consistent with the scenario for the pure Mg cluster. The dopant of Sr usually occupies the convex capped sites of the $SrMg_n^{0/-}$ cluster. The analysis of the difference between the binding energy and the second-order energy shows that the $SrMg_9^{0/-}$ cluster with tower framework has outstanding stability. The molecular orbital and chemical bonding analysis indicate that the stronger Sr–Mg interaction leading to the sp hybridization between Sr and Mg atoms can stabilize the $SrMg_9$ cluster.

Acknowledgements

Project supported by the National Natural Science Foundation of China (Grant No. 11404008), the Artificial Intelligence Key Laboratory of Sichuan Province, China (Grant No. 2018RYJ07), the Innovation Fund of Postgraduate Sichuan University of Science & Engineering, China (Grant Nos. y202007 and y2021008), the Innovation and Entrepreneurship Training Program of Sichuan Province, China (Grant Nos. S202010622080 and S202010622082), and the Innovation and Entrepreneurship Training Program of Sichuan University of Science & Engineering, China (Grant No. cx2019005).

The computation of this work was completed at Sichuan University of Science & Engineering High Performance Computing Center of Science & Engineering.

References

[1] Akola J, Rytkönen K and Manninen M 2001 *Eur. Phys. J. D* **16** 21
[2] Köhn A, Weigend F and Ahlrichs R 2001 *Phys. Chem. Chem. Phys.* **3** 711
[3] Jellinek J and Acioli P H 2002 *J. Phys. Chem. A* **106** 10919
[4] Thomas O C, Zheng W, Xu S, Bowen K H and Shiloh J M 2002 *Phys. Rev. Lett.* **89** 213403
[5] Janecek S, Krotscheck E, Liebrecht M and Wahl R 2011 *Eur. Phys. J. D* **63** 377
[6] Xia X X, Hermann A, Kuang X Y, Jin Y Y, Lu C and Xing X D 2016 *J. Phys. Chem. A* **120** 7947
[7] Belyaev S N, Panteleev S V, Ignatov S K and Razuvaev A G 2016 *Comput. Theor. Chem.* **1079** 34
[8] Axel B D 1998 *J. Chem. Phys.* **98** 5648
[9] Li Y S, Sun L X, Zhou X, Chen K and Wang H Y 2020 *Acta Phys. Sin.* **69** 013101 (in Chinese)
[10] Cai M Y, Tang C M and Zhang Q Y 2019 *Acta Phys. Sin.* **68** 213601 (in Chinese)
[11] Yin M, Zhang M, Lü J and Wu H S 2019 *Acta Phys. Sin.* **68** 203102 (in Chinese)
[12] Wang S J, Kuang X Y, Lu C, Li Y F and Zhao Y R 2011 *Phys. Chem. Chem. Phys.* **13** 10119
[13] Kuang X J, Wang X Q and Liu G B 2013 *J. Alloys Compd.* **570** 46
[14] Zhu B C, Zhang S and Zeng L 2020 *Int. J. Quantum Chem.* **120** e26143
[15] Zhang F G, Zhang H R, Xin W, Chen P, Hu Y F and Zhao Y R 2020 *Sci. Rep.* **10** 6052
[16] Kang D L, Sun W G, Shi H X, Lu C, Chen B L and Maroulis G 2019 *Sci. Rep.* **9** 14367
[17] Xu K M, Huang T, Liu Y R, Jiang S, Zhang Y, Lv Y Z, Gai Y B and Huang W 2015 *Chem. Phys.* **456** 13
[18] Li J, Liu X Y, Zhu Z H and Sheng Y 2012 *Chin. Phys. B* **21** 33101
[19] Zhang J T, Li J and Sheng Y 2014 *Chin. Phys. B* **23** 013103
[20] Shi S P, Zhang C Y, Zhao X F, Li X, Yan M and Jiang G 2017 *Chin. Phys. B* **26** 083103
[21] Gu X N, Xie X H, Li N, Zheng Y F and Qin L 2012 *Acta Biomater.* **8** 2360
[22] Bornapour M, Mahjoubi H, Vail H, Shum-Tim D and Pekgieryuz 2016 *Mater. Sci. Eng. C* **67** 72
[23] Wang Y C, Lv J, Li Z and Ma Y 2012 *Comput. Phys. Commun.* **183** 2063
[24] Wang Y C, Miao M S, Lv J, Zhu L, Yin K, Liu H and Ma Y 2012 *J. Chem. Phys.* **137** 224108
[25] Zhang X Y, Qin J Q, Sun X W, Xue Y N and Liu R P 2013 *Phys. Chem. Chem. Phys.* **15** 20894
[26] Zhang M G, Yan H Y, Wei Q and Wang H 2013 *Comput. Mater. Sci.* **68** 371
[27] Ju M, Lv J, Kuang X Y, Ding L P and Maroulis G 2014 *RSC Adv.* **5** 6560
[28] Yang C, Jia S H, Ma M F, Zhang S, Lu C and Li G Q 2015 *Eur. Phys. J. D* **69** 244
[29] Li C G, Li H J, Cui Y Q, Tian H, Shao Q Q, Zhang J, Zhao G, Ren B Z and Hu Y F 2021 *J. Mol. Liq.* **339** 116764
[30] Li C G, Shen Z G, Zhang J, Cui Y Q, Li J J, Xue X Y, Li H F, Ren B Z and Hu Y F 2020 *New J. Chem.* **44** 5109
[31] Tian Y H, Sun W G, Chen B L, Jin Y Y and Lu C 2019 *Chin. Phys. B* **28** 103104
[32] Li L, Cui X H, Cao H, Cao H B, Jiang Y, Duan H M, Jing Q, Liu J and Wang Q 2020 *Chin. Phys. B* **29** 077101
[33] Hay P J and Wadt W R 1985 *J. Chem. Phys.* **82** 299
[34] Krishnan R, Binkley J S, Seeger R and Pople J A 1980 *J. Chem. Phys.* **72** 650
[35] Frisch M J, Trucks G W, Schlegel H B, *et al*. 2013 Gaussian 09, Revision D.01; Gaussian, Inc., Wallingford CT
[36] Fuentealba P, Szentpaly L V and Preuss H 1985 *J. Phys. B: At. Mol. Phys.* **18** 1287
[37] Akola J, Manninen M and Häkkinen H 1999 *Phys. Rev. B* **60** R11297
[38] Lu T and Chen F 2012 *J. Comput. Chem.* **33** 580
[39] Zubarev D Y and Boldyrev A I 2008 *Phys. Chem. Chem. Phys.* **10** 5207
[40] Acioli P H and Jellinek J 2002 *Phys. Rev. Lett.* **89** 213402
[41] Lyalin A, Solov'yov I A, Solov'yov A V and Greiner W 2003 *Phys. Rev. A* **67** 063203
[42] Heidari I, De S, Ghazi S M, Goedecker S and Kanhere D G 2011 *J. Phys. Chem. A* **115** 12307
[43] Zhao Y R, Zhang H R, Qian Y, Duan X C and Hu Y F 2015 *Mol. Phys.* **114** 784
[44] Xing X D, Wang J J, Kuang X Y, Xia X X, Lu C and Maroulis G 2016 *Phys. Chem. Chem. Phys.* **18** 26177
[45] Issendorff B V and Cheshnovsky O 2005 *Ann. Rev. Phys. Chem.* **56** 549
[46] Xia X X, Hermann, Kuang X Y, Jin Y Y, Lu C and Xing X D 2015 *J. Phys. Chem. C* **120** 677
[47] Zhang J M, Duan Y N, Xu K W, Ji V and Man Z Y 2008 *Physica B* **403** 3119
[48] Jin S Y, Chen B L, Kuang X Y, Lu C and Gutsev G L 2019 *J. Phys.: Condes. Matter* **31** 485302
[49] Ding L P, Kuang X Y, Shao P, Zhao Y R and Li Y F 2012 *Chin. Phys. B* **21** 043601
[50] Zhao Y R, Zhang H R, Zhang M G, Zheng B B and Kuang X Y 2013 *Mol. Phys.* **112** 972
[51] De S, Ghasemi S A, Willand A, Genovese L, Kanhere D and Goedecker S 2011 *J. Chem. Phys.* **134** 124302
[52] Kong F J and Hu Y F 2014 *J. Mol. Model.* **20** 2087
[53] Zhao Y R, Kuang X Y, Shao P, Li C G, Wang S J and Li Y F 2012 *J. Mol. Model.* **18** 1333
[54] Sun H R, Kuang X Y, Li Y F, Shao P and Zhao Y R 2012 *Chin. Phys. B* **21** 083601
[55] Zhang S, Jiang H L, Wang P, Lu C, Li G Q and Zhang P 2013 *Chin. Phys. B* **22** 123601
[56] Zhang S, Zhang Y, Yang Q X, Li G Q and Lu Z W 2019 *New J. Chem.* **43** 10030
[57] Zhang L H, Xia X X, Sun W G, Lu C, Kuang X Y, Chen B L and Maroulis G 2018 *Sci. Rep.* **8** 6702
[58] Zhao Y R, Xu Y Q, Chen P, Yuan Y Q, Qian Y and Li Q 2021 *Results Phys.* **26** 104341
[59] Reed A E, Weinstock R B and Weinhold F 1985 *J. Chem. Phys.* **83** 735